

Three-dimensional bead position histograms reveal single-molecule nanomechanicsNils B. Becker,^{1,*} Stephan M. Altmann,² Tim Scholz,³ J. K. Heinrich Hörber,⁴ Ernst H. K. Stelzer,¹ and Alexander Rohrbach^{1,†}¹*European Molecular Biology Laboratory, Meyerhofstraße 1, 69117 Heidelberg, Germany*²*BASF AG, Carl-Bosch-Straße 38, 67056 Ludwigshafen, Germany*³*Medizinische Hochschule Hannover, Carl-Neuberg-Straße 1, 30625 Hannover, Germany*⁴*Wayne State University, Detroit, Michigan 48202, USA*

(Received 12 July 2004; published 22 February 2005; corrected 28 February 2005)

We describe a method to investigate the structure and elasticity of macromolecules by a combination of single molecule experiments and kinematic modeling. With a photonic force microscope, we recorded spatial position histograms of a fluctuating microsphere tethered to full-length myosin-II. Assuming only that the molecule consists of concatenated rigid segments, a model derived from robot kinematics allows us to relate these histograms to the molecule's segment lengths and bending stiffnesses. Both our calculated position distributions and the experimental data show an asymmetry characteristic of a mixed entropic-enthalpic spring. Our model that fits best to experimental line profiles has two intramolecular hinges, one at the bound head domain, and another about 50 nm down the myosin tail, with a summed bending stiffness of about $3 k_B T/\text{rad}$.

DOI: 10.1103/PhysRevE.71.021907

PACS number(s): 87.15.La, 87.15.Aa, 87.15.Ya, 87.80.Cc

I. INTRODUCTION

In the study of motor molecules, optical single molecule techniques have been widely used to measure properties of the mechanochemical cycle, such as step size and load-dependent speed [1–3]. Motor function depends on ATPase activity at the head domains of the protein. However, any force acting at the head domain in such experiments is balanced by the elastic response of the whole molecular construct used. The tail elasticity therefore influences the statistics of the force and torque that act at the head domains of the molecule. Also for myosin function in muscle [4,5], the passive elasticity of the myosin cross bridge is essential. To understand the mechanochemical cycle in depth, it seems important to characterize the passive elastic response of the complete motor molecules including the tail domains. The analysis of three-dimensional (3D) elastic properties of rodlike single macromolecules is also interesting as a test of polymer physics models and for nanotechnology applications.

These elastic properties can be measured in single-molecule experiments [6] using a photonic force microscope (PFM) [7,8]. Here, a submicrometer-sized bead is tethered to a coverslip by a single rodlike molecule and confined in a weak optical trap. The bead explores the local free energy landscape by thermal motion, while its 3D position is recorded interferometrically. The spatial resolution of the position histogram achieved is on the order of 2–5 nm in 3D with a sampling rate higher than 100 kHz. Since the bead moves diffusively in a predefined volume, it will probe the tether elasticity in a wide range of directions and on multiple time scales at once, in contrast to the situation using atomic force microscopy or conventional optical tweezers. By re-

ording histograms of the bead position, an energy resolution on the order of $0.1 k_B T$ can be achieved, depending on bin size and recording time. Another method that can provide 2D [9,10] or 3D [11] position histograms is video tracking, but with a lower temporal resolution in the millisecond range, leading to motion blur for fast fluctuations of small trapped beads and thereby limiting the spatial resolution. To relate the measured histograms to molecular elasticity, a model for the mechanics of the bead-molecule tether is required. The simplest assumption of a swiveling, radial Hookean spring [6,12] with a rigidly attached bead fails to account for the experimentally observed asymmetry in radial line profiles (see below). To explain this asymmetry, the internal nanomechanics of the molecule has to be taken into account.

One possible model for the tail of a rodlike motor molecule such as conventional kinesin or myosin-II is a semiflexible polymer, e.g., a wormlike chain (WLC) [13], characterized by a contour length and a persistence length l_p . This corresponds to a uniform distribution of bending compliance along the molecule. There is evidence from structural and electron-microscopy studies, however, that the tail region of kinesin can bend strongly at a single point about midway along the tail [14]. Also, myosin-II can be enzymatically split into heavy (HMM) and light meromyosin (LMM) at a point on the tail about 50 nm from the head domain, indicating an interruption of the regular coiled-coil structure [15]. Therefore, a complementary description is considered here; in the opposite limit of maximally concentrated bending compliance, one obtains a *segmentally flexible* molecule with a few rigid subunits connected by pointlike joints. This view is supported by a molecular dynamics study of the leucine zipper of the SNARE complex, which indicated a high rigidity for this structurally similar coiled-coil domain [16].

In the present article, we describe a mechanical model for the passive elastic properties of segmentally flexible, rodlike macromolecules attached to a single bead. In Sec. II a mathematical framework [17] is introduced to conveniently describe the relative configurations of the rigid segments of

*Electronic address: nbecker@mpipks-dresden.mpg.de

†Electronic address: rohrbach@embl.de

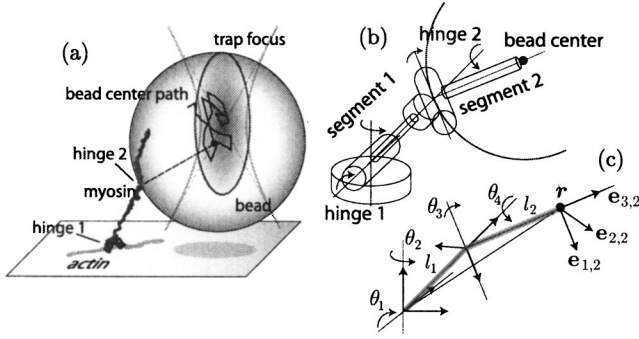


FIG. 1. (a) An actin-myosin molecular tether, with a short segment of the Brownian bead center trajectory. (b) The same system represented as a robot arm with two segments and four joint angles. (c) The corresponding kinematic chain with reference frames attached to each link. The last link corresponds to a bead radius from the binding point to the bead center. Here, spherical coordinates are chosen as joint angles $\{\theta_i\}$.

such a molecule, and a general strategy to obtain the stationary 3D bead position distribution is outlined. This strategy is then carried out in Sec. III for the case of a molecule with isotropic bending stiffness and no intrinsic curvature. Generic results for a molecule with one and two segments are shown in Sec. IV. We then compare the model to experimental data [18] obtained from full-length myosin-II (Sec. V). The model reproduces the radial asymmetry observed experimentally in a natural way, if the segment subdivision is chosen appropriately.

II. CALCULATION OF 3D DISTRIBUTIONS

A typical experimental assay is depicted in Fig. 1(a). A rodlike macromolecule, e.g., myosin-II, is attached at one end to an actin filament adhering to the coverslip, and to a bead of 100–500 nm diameter at the other. The bead is trapped in 3D in a weak optical trap. The random trajectory of the bead is recorded in 3D with the PFM with a sampling rate and bandwidth of 100 kHz. An estimate of the bead's position autocorrelation time gives $\tau = \gamma(\Delta z^2)/k_B T \approx 3$ ms, where γ is the Stokes viscous drag of the bead at room temperature. So the bead trajectory can be time resolved with the setup. Bead position histograms of such trajectories reflect an effective free energy landscape for the bead resulting from the molecule and the optical trap.

Do such histograms contain any information about the molecule, considering that the bead is larger in volume than the molecule by three orders of magnitude? The bead mass is irrelevant, since the system is overdamped. Also, the bead-coverslip interaction has a range of only a few nanometers at experimental salinity. When the trapping laser is dimmed so that the optical trap stiffness is lower than molecular elastic stiffness constants, the attached bead will thus have two main effects: Slowed-down diffusion, which allows for adiabatic thermal averaging over the internal conformational degrees of freedom of the molecule, and volume exclusion, which restricts the accessible range of the system. In this regime, the bead position distribution is determined mainly by elastic

properties of the molecule, in the geometrically allowed range.

A segmentally flexible linear polymer with a bead attached on one end and bound to the coverslip on the other end will be called a *molecular tether* (MT). An inextensible MT can be modeled as a kinematic chain: Rigid links (the segments) are connected by pointlike rotational joints, which represent the hinge regions of the molecule. The last link corresponds to the line from the bead-molecule binding point to the bead center, indicated by the dashed line in Fig. 1(a). The bead radius is thus incorporated in the MT, including bead size effects in our analysis. The resulting picture is analogous to a *robot arm* with n links of lengths $\{l_i\}_{1 \leq i \leq n}$ and $m(m \geq n)$ rotational joint angles, Fig. 1(b). For full orientation freedom, three rotational joint axes are needed between any two adjacent links, intersecting at the hinge point.

As a preliminary step, we introduce a group formalism [17,19] used in robot kinematics that is suited to relate the bead center position $\mathbf{r} = (r_1, r_2, r_3)$ to the joint angles.

Let $(\mathbf{e}_{1,0}, \mathbf{e}_{2,0}, \mathbf{e}_{3,0})$ denote a right-handed orthonormal reference frame (*frame*) fixed to the coverslip, with its origin \mathbf{p}_0 at the starting point of the first link, the *base frame*. Also fix a frame $(\mathbf{e}_{1,i}, \mathbf{e}_{2,i}, \mathbf{e}_{3,i})$ to the end point \mathbf{p}_i of the i th link, $1 \leq i \leq n$, such that $\mathbf{e}_{3,i}$ points in the direction of the i th link, i.e., $\mathbf{e}_{3,i} \parallel (\mathbf{p}_i - \mathbf{p}_{i-1})$, Fig. 1(c). So the *backbone* of the molecule is given by the sequence of the $\{\mathbf{p}_i\}$. Let $(\cdots)_j$ denote coordinates relative to frame j . The 4×4 (block) matrix

$$\underline{g}_{ji} = \begin{pmatrix} \mathbf{e}_{1,i} & \mathbf{e}_{2,i} & \mathbf{e}_{3,i} & \mathbf{p}_i \\ 0 & 0 & 0 & 1 \end{pmatrix}_j = \begin{pmatrix} \underline{R}_i & \mathbf{p}_i \\ \mathbf{0}^T & 1 \end{pmatrix}_j, \quad (1)$$

describes the *configuration* of frame i relative to frame j . Here, $(\mathbf{p}_i)_j$ and the rotation matrix $(\underline{R}_i)_j$ describe the position and orientation, respectively. \underline{g}_{ji} is an element of the homogeneous representation of the Lie group SE(3) of rigid motions in Euclidean space. Define 3×3 antisymmetric matrices $\underline{\epsilon}_p$ in terms of the antisymmetric tensor by $(\underline{\epsilon}_p)_{q,r} = \epsilon_{pqr}$. For example, $\underline{\epsilon}_3$ generates a rotation about the z axis. The Lie algebra $\mathfrak{se}(3)$ corresponding to SE(3) can be represented in terms of 4×4 *twist matrices*

$$\underline{\xi}(\mathbf{v}, \boldsymbol{\omega}) = \begin{pmatrix} -\sum_{p=1}^3 \omega_p \underline{\epsilon}_p & \mathbf{v} \\ \mathbf{0}^T & 0 \end{pmatrix}; \quad \mathbf{v}, \boldsymbol{\omega} \in \mathbb{R}^3. \quad (2)$$

Any twist matrix generates a combined rotation and translation (a *screw motion*) via the matrix exponential. As can be shown [17], a pure rotation about a fixed axis going through any point \mathbf{q} in a direction $\boldsymbol{\omega}$, $\|\boldsymbol{\omega}\|=1$, is generated by the twist $\underline{\xi}_{rot} = \underline{\xi}(\mathbf{q} \times \boldsymbol{\omega}, \boldsymbol{\omega})$. By the group property of the \underline{g}_{ji} , to obtain the end frame configuration \underline{g}_{0n} , one just multiplies the homogeneous matrices corresponding to the joints along the kinematic chain, ordered for increasing joint number. The end frame configuration \underline{g}_{0n} of a robot arm can then be given in terms of the joint angles $(\theta_1, \dots, \theta_m)$ by the *product-of-exponentials* (POE) formula [20]

$$\underline{g}_{0n}(\theta_1, \dots, \theta_m) = \exp[\underline{\xi}_1 \theta_1] \cdots \exp[\underline{\xi}_m \theta_m] \underline{g}_{0n}(0, \dots, 0). \quad (3)$$

Here, for each joint number k , $1 \leq k \leq m$, ξ_k denotes the *constant* twist ξ_{rot} associated with the joint axis, given in base frame coordinates, and evaluated in the *reference configuration*, i.e., with all joint angles set to 0. It will be chosen linear and untwisted.

We now outline how to calculate the spatial bead center probability density function (PDF) using this framework.

Given an angular potential $V(\theta_1, \dots, \theta_m)$, the PDF in the space of joint angles is given by a Boltzmann factor $e^{-V/k_B T}$. To obtain the spatial PDF $p(\mathbf{r})$, internal motions of the chain have to be made explicit and then integrated over. More specifically, we need to find a coordinate transformation T , so that $(\tilde{\theta}_1 \equiv r_1, \tilde{\theta}_2 \equiv r_2, \tilde{\theta}_3 \equiv r_3, \tilde{\theta}_4, \dots, \tilde{\theta}_m) = T^{-1}(\theta_1, \dots, \theta_m)$ is a new set of coordinates that contains $\mathbf{r} = (r_1, r_2, r_3)$. Then in the new variables the PDF is given by

$$p(\tilde{\theta}_1, \dots, \tilde{\theta}_m) d^m \tilde{\theta} \propto e^{-(1/k_B T)V(T(\tilde{\theta}_1, \dots, \tilde{\theta}_m))} \times A(T(\tilde{\theta}_1, \dots, \tilde{\theta}_m)) \times |DT(\tilde{\theta}_1, \dots, \tilde{\theta}_m)| d^m \tilde{\theta}, \quad (4)$$

where $|DT|$ is the absolute value of the functional determinant of T , and $Ad^m \theta$ is the volume element in the (old) joint angle space. The 3D bead center PDF is then a marginal distribution when integrating over the internal variables (a partial trace), i.e.,

$$p(r_1, r_2, r_3) \propto \int_{\mathcal{R}(\mathbf{r})} p(\tilde{\theta}_1, \dots, \tilde{\theta}_m) d\tilde{\theta}_4 \cdots d\tilde{\theta}_m. \quad (5)$$

The integration domain $\mathcal{R}(\mathbf{r})$ for internal motions depends on the bead center position due to the inextensibility of the MT. It is this varying volume of internal configuration space that generates entropic elasticity in the model.

For general kinematic chains, it is a difficult task to find T explicitly, related to the inverse kinematics problem in robot kinematics. In what follows, an n -segment MT with a stretched-out minimum energy configuration and direction-independent bending stiffness will be considered. For this simple MT geometry, T and \mathcal{R} can be determined analytically, using the POE formula recursively, to give the spatial PDF.

III. APPLICATION

As a minimal model, we consider a segmentally flexible molecule in which each hinge is a very short elastic rod with no intrinsic curvature or torsion. Although the myosin tail adheres tangentially to the bead surface over some fraction of its length [18], this strong adhesion likely denatures the coiled-coil structure of the myosin tail locally. Therefore, the assumption of no intrinsic bending is justified as a minimal choice also for the last link of the MT.

Then, ZYZ Euler angles $(\varphi_i, \vartheta_i, \gamma_i)$ are suited to reflect the total bend ϑ_i of the hinge, and its total twist $\varphi_i + \gamma_i$. Here, (φ_i, ϑ_i) are standard spherical angles, while γ_i describes the final Z' rotation of the segment i . For an ideal elastic rod with isotropic bending stiffness, a harmonic, uncoupled approximation for the angular potential is

$$V = \sum_{i=1}^n \frac{1}{2} \kappa_{b,i} \vartheta_i^2 + \frac{1}{2} \kappa_{tw,i} (\varphi_i + \gamma_i)^2, \quad (6)$$

with twisting and bending stiffnesses $\kappa_{tw,i}$ and $\kappa_{b,i}$, respectively. To account for volume exclusion between molecule and bead or coverslip, the ranges of ϑ_1 and ϑ_n are restricted to $(0, \pi/2)$, while between two inner segments $\vartheta_j < \pi$. The repulsive bead-coverslip interaction is implemented as a short-ranged exponential in position space.

Note that the number of relevant joint variables is only $2n$. Intuitively, since the bead orientation \underline{R}_{0n} is not measured, motions that leave the backbone fixed will relax any twist along the molecule undetected. By using the corresponding POE, it can be shown that the joint angles enter into $p(\mathbf{r})$ only through the combinations $\{\vartheta_i, \eta_i^+ = \gamma_{i-1} + \varphi_i\}_{1 \leq i \leq n}$, where $\gamma_0 = 0$, and that the twist stiffnesses $\kappa_{tw,i}$ do not enter at all. This is only the case since we exclude intrinsic kinks along the chain.

The resulting end frame configuration $\underline{g}_{0n}(\eta_1^+, \vartheta_1; \dots; \eta_n^+, \vartheta_n)$ is given by the POE (*ordered for increasing i*)

$$\underline{g}_{0n} = \prod_{i=1}^n \exp[\underline{\xi}(\mathbf{0}, \hat{\mathbf{z}}) \eta_i^+] \exp[\underline{\xi}(-L_{i-1} \hat{\mathbf{x}}, \hat{\mathbf{y}}) \vartheta_i] \begin{pmatrix} \frac{1}{\mathbf{0}^T} & L_n \hat{\mathbf{z}} \\ \mathbf{0} & 1 \end{pmatrix}, \quad (7)$$

where $\hat{\mathbf{x}} = (1, 0, 0)^T$, etc., $L_k = \sum_{i=1}^k l_i$, and the last matrix defines the stretched reference configuration. The corresponding angular PDF is

$$p(\eta_1^+, \vartheta_1; \dots; \eta_n^+, \vartheta_n) d^m \theta \propto \prod_{i=1}^n \sin(\vartheta_i) e^{-\kappa_{b,i} \vartheta_i^2 / 2k_B T} d\vartheta_i d\eta_i^+. \quad (8)$$

The volume factor $A = \prod_i \sin \vartheta_i$ in the joint angle space gives a uniform distribution of directions at each hinge in the high-temperature limit.

We now sketch how a new set of $2n$ variables $(r_1, r_2, r_3; \tilde{\vartheta}_1, \tilde{\varphi}_1; \dots; \tilde{\vartheta}_{n-3}, \tilde{\varphi}_{n-3}; \tilde{\varphi}_{n-2})$ can be recursively determined to separate the bead center position \mathbf{r} from the internal motions of the MT. These together with the transformation T then allow us to calculate $p(\mathbf{r})$ via Eqs. (4) and (5). Each recursive step consists of two substeps: rotation of the link i from the reference configuration to the direction of the end point (the bead center), followed by rotation into the final orientation. The new variables $(\tilde{\vartheta}_i, \tilde{\varphi}_i)$ are defined as the standard spherical angles that describe the second substep at each joint except for the last. This procedure generates the transformation T and gives an explicit formula for $\mathcal{R}(\mathbf{r})$ (not shown).

IV. RESULTS

The algorithm described in the previous section was implemented in MATHEMATICA for two- and three-link chains, using packages from [17]. Integration over the internal motions of the chain was done numerically. We obtain

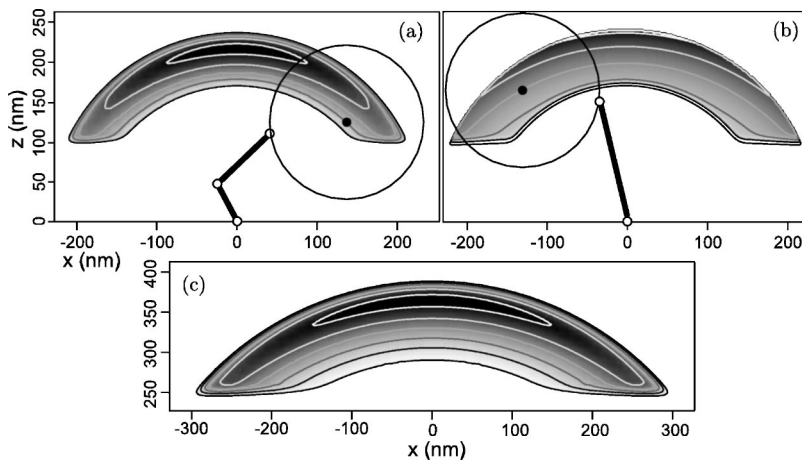


FIG. 2. Slices through the calculated 3D bead center PDF in the x - z plane, for two and three links at constant molecule length. Bead radius 100 nm in (a),(b) and 250 nm in (c). Contour lines are for equidistant PDF levels. Other parameters are (a) and (c) $(l_1, l_2) = (50, 90)$ nm, $(\kappa_1, \kappa_2, \kappa_3) = (0.6, 2.0, 1.5)k_B T/\text{rad}$; (b) $l_1 = 140$ nm, $(\kappa_1, \kappa_2) = (0.6, 0.8)k_B T/\text{rad}$.

spatial PDFs that are rotationally symmetric with respect to the $\mathbf{e}_{3,0}$ axis. The $\mathbf{e}_{i,0}$ axes will be identified with space-fixed x , y , and z axes in the following. In Fig. 2, 2D slices through some calculated 3D PDFs $p(\mathbf{r})$ of the bead center are shown. The outer radius is L_n , while the inner radius depends on the maximally allowed bending angles.

The two-link PDFs are peaked on the outer rim for bending stiffnesses higher than $\approx 0.1k_B T/\text{rad}$. This is not true in the three-link case due to an increased entropic contribution. This feature is clearly visible in line profiles of the 3D bead center PDF along the z axis. For two links (Fig. 3, inset), the profile sharply drops to 0 at maximum extension. When Gaussian smoothing is included (Fig. 3) to mimic the position measurement error, the peak remains within 10 nm of the outer rim, essentially independent of stiffness. This is also true in the three-link case with a strongly asymmetric $(l_1, l_2) = (10, 130)$ nm subdivision of the molecule (Fig. 4, inset). The latter MT geometry corresponds to a myosin molecule with flexible S1-S2 junction and a tail that is stiff over its whole length. Conversely, a more symmetric $(l_1, l_2) = (50, 90)$ nm MT subdivision corresponds to a flexible hinge at the HMM-LMM junction midway along the myosin tail, and no S1-S2 compliance. In this case, the skewness of the

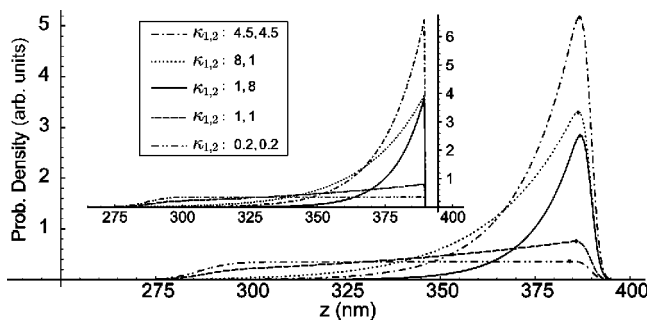


FIG. 3. Calculated z -axis line profiles of the 3D bead center PDF of the two-link model with $(l_1, l_2) = (140, 250)$ nm for varying total stiffness and stiffness distribution. The profiles were smoothed with a Gaussian of full width at half maximum 4 nm, corresponding to the experimental position measurement uncertainty. The PDFs are normalized in 3D. Inset: The nonsmoothed profiles, exhibiting a discontinuity at the outer rim. Bending stiffnesses are given in $k_B T/\text{rad}$.

line profile becomes less pronounced as the PDF peak moves inward when the total stiffness decreases (Fig. 4). Generally, the three-link profiles become more skewed with increasing total stiffness and with increasing asymmetry of the molecule subdivision.

Since the distributions are normalized in 3D, the varying area under the shown radial line profiles reflects the width of the distribution in the lateral direction. High total stiffness results in a laterally confined bead movement with high probability close to the z axis. In Fig. 5, radial line profiles with a constant total stiffness of $9k_B T/\text{rad}$ are shown, comparable to the experimental value. Their area variation is less pronounced than in Fig. 4, showing that the lateral confinement depends rather weakly on the distribution of stiffness among the three joints. For the geometry shown there, the stiffness κ_3 characterizing the bond of the molecule tail to the bead, has the biggest influence, since it connects the two longest links in the chain. Low κ_3 leads to an elevated tail on the inner side of the distribution. This is also true for κ_2 in the two-link case (Fig. 3).

V. COMPARISON WITH EXPERIMENTAL DATA

Single-molecule PFM experiments as described above were done on full-length myosin-II from rabbit *psoas*

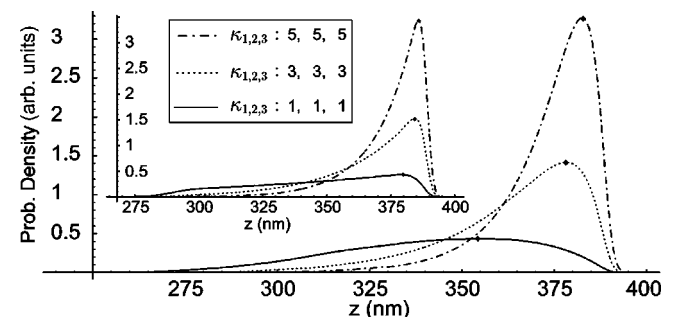


FIG. 4. Calculated z -axis line profile of the 3D bead center PDF of the three-link model, Gaussian smoothed, for varying total stiffness and with $(l_1, l_2, l_3) = (50, 90, 250)$ nm. Inset: The same plot with $(l_1, l_2, l_3) = (10, 130, 250)$ nm. A clear dependence of the peak location on the total stiffness can be seen only in the case of a hinge near the midpoint of the molecule.

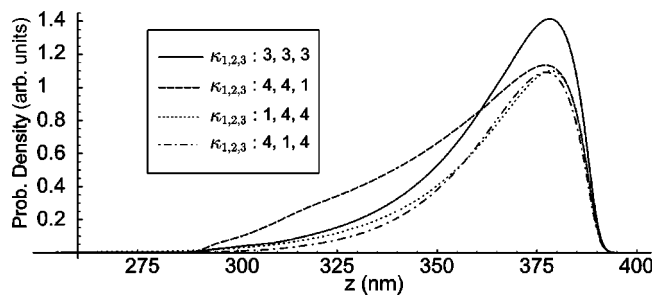


FIG. 5. Calculated z -axis line profiles of the 3D bead center PDF of the three-link model, Gaussian smoothed, for constant total stiffness, but varying stiffness distribution. The peak location is independent of the stiffness distribution; only the tail shape on the inner side varies appreciably. $(l_1, l_2, l_3) = (50, 90, 250)$ nm.

muscle, which was bound to actin filaments in the rigor state. Although no attempt was made to measure stiffness constants, the data support the picture of a MT with a mixed enthalpic-entropic spring and provide constraints on the relevant link lengths.

Microspheres with a diameter of 500 nm were sparsely coated with myosin molecules, and after trap calibration [7,22] were tethered to immobilized actin filaments in ATP-free solution. When a specific binding event occurred, time traces of the 3D bead position were recorded for a time of up to one minute. A binding event was indicated by a sudden restriction of the volume of diffusion. For a trap positioned roughly over the tether base, this restriction occurs almost exclusively in the z direction, where the molecule stiffness is highest and the trap stiffness is lowest (Fig. 6). After initial binding, the position of the optical trap was scanned in the x and y directions, which allowed us to verify the presence of a single MT and to exclude surface interaction as the origin

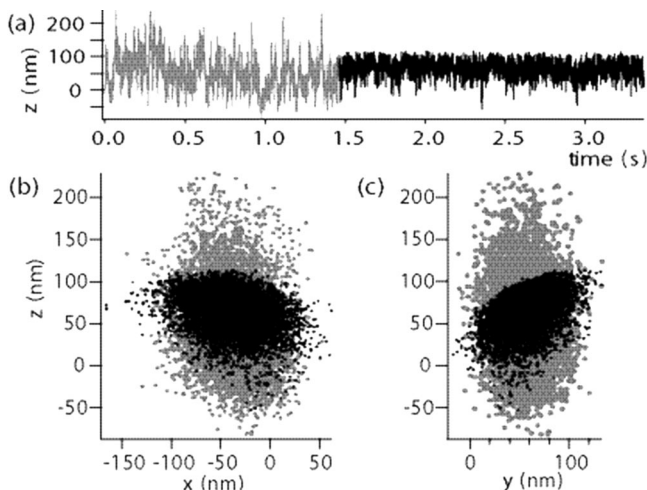


FIG. 6. Measured time trace of the z -position signal (a) and the point cloud from the same data, projected onto the x - z and y - z planes (b) and (c). The initial binding event is clearly visible at $t \approx 1.5$ s. Note that diffusion becomes additionally restricted in the z direction but not in the x - y plane upon binding. The binding point on the coverslip is slightly offset in the negative x and positive y directions.

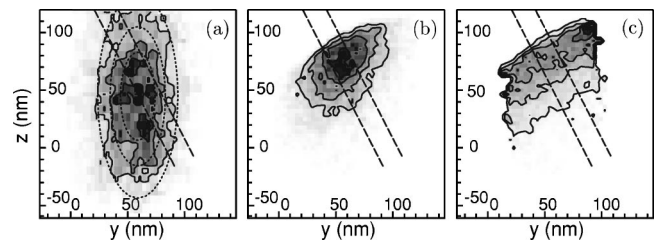


FIG. 7. y - z slices through measured 3D histograms of the data shown in Fig. 6, before (a) and after (b) binding. Pointwise division of (b) by a Gaussian fit (dotted ellipses) to (a) gives the histogram (c), corresponding to $p(\mathbf{r})$. Black represents 180 (a) and 280 (b) counts; bin size was $4.8 \times 3.5 \times 3.6$ nm³. Contour lines are for equidistant PDF levels; all histograms were thresholded at 15 counts. Dashed lines indicate the region averaged in the line profiles.

of the observed traces. Furthermore, the binding of actin to the coverslip is about 100 times stiffer than our observed z direction stiffness constants, as can be checked by directly binding beads to immobilized actin with a biotin-streptavidin link (for experimental details see [18]).

As can already be seen from Fig. 6, confinement is mainly trap induced in the lateral directions, while in the z direction it is caused by the MT. Here, the optical trap is weaker than the elastic tether forces and thus the complete z range accessible to the MT can be seen at a fixed trap position. However, the trapping force cannot be completely neglected. To obtain a histogram corresponding to the calculated MT PDF p , we assume that the trap and the MT act like additive spatial potentials. This assumption is well justified since the internal motions of the molecule are fast compared to the bead motion and since the optical trap's scattering force [21] is approximately position independent. The trap PDF p_{trap} and the MT PDF p then multiply to give the observed total PDF

$$p_{\text{bound}}(\mathbf{r}) \propto p(\mathbf{r})p_{\text{trap}}(\mathbf{r}). \quad (9)$$

Figure 7(c) shows the histogram corresponding to $p(r)$, calculated by pointwise division according to Eq. (9). A Gaussian fit corresponding to the harmonic trapping potential was used for p_{trap} instead of the measured histogram in Fig. 7(a), as no surface interaction effects were visible. Although not necessary here, we note that the division procedure can also be used to correct for additive potentials of arbitrary shape, e.g., remaining unspecific surface interactions, given a measurement apparatus with sufficiently low drift. The corrected "MT-only" histogram in Fig. 7(c) exhibits parallel contour lines indicating a deflection angle from the z axis of about 30°. In the direction normal to the contours, the histogram is peaked toward the outer rim of the accessible range. This asymmetry in radial direction was observed in many trials and rules out the simple assumption of a radial linear spring as the elastic element of the tether.

Line profiles of the measured histograms are shown in Fig. 8. The radial asymmetry seen in the raw data of the bound bead is preserved when correcting for the trap influence. Specifically, the softer slope of the distribution towards the coverslip does not result from the optical trap or from surface interaction. The MT clearly is weakly repulsive at

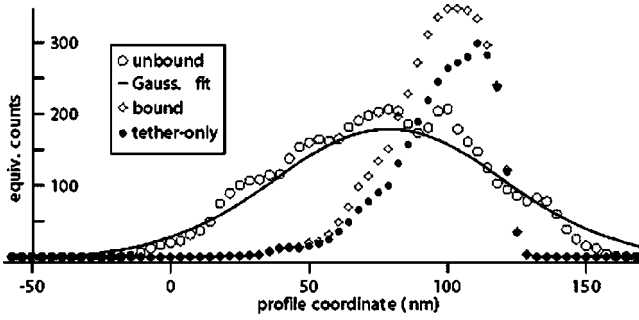


FIG. 8. Radial profiles as indicated in Fig. 7 by the dashed lines, for the unbound [7(a)], bound [7(b)], and “MT-only” [7(c)] histograms, respectively. Note the strong concentration toward the outer rim of the distribution. Profiles were averaged over a linewidth of five bins and rescaled such that the equivalent count number has a Poisson-like error given by the square root.

low elongation and strongly attractive at high elongation, a hallmark of a mixed enthalpic-entropic spring.

Fits were attempted for a total linker length of 110 nm corresponding to the maximum width of the tether-only profile, Fig. 8. In the case of the three-link model, subdivisions of the molecule at 10 and at 50 nm from the base were compared, roughly matching the lever arm length proposed for the power stroke [22,23], and the supposed region of increased compliance at the HMM-LMM junction [15], respectively. The least-squares fits of the two-link and asymmetrically subdivided three-link models are clearly inadequate, Fig. 9. They overestimate the attractive stiffness and underestimate the repulsive stiffness of the molecule. However, when l_1 in the three-link model is increased to a value of 50 nm, a good fit to the data can be achieved. The resulting κ_3 value suggests that the bead is rather rigidly bound. While the exact distribution of stiffness among the intramolecular hinges κ_1 – κ_2 is not determined reliably due to its small influence on the histogram (see Fig. 5), the total stiffness value $\kappa_1 + \kappa_2$ is around $3.4k_B T$.

VI. DISCUSSION

The three-link model for the MT constitutes the simplest kinematic chain with rigid subunits that is consistent with the experimentally observed z -direction line profiles. It has isotropic bending symmetry which eliminates the twist stiffnesses. This leaves six model parameters: the link lengths $\{l_i\}$ and the bending stiffnesses $\{\kappa_i\}$. This number can be further reduced. The bead radius l_3 may be determined independently, and the total molecule length $l_1 + l_2$ can be fixed by the total width of the radial line profile. Of the remaining four parameters, the total stiffness $\Sigma \kappa_i$ determines the peak sharpness of the PDF, while the peak position or skewness is controlled by the quantity $l_2 - l_1$. The distribution of bending stiffness among the joints can be roughly determined using its small effect on the PDF (see Fig. 5) by considering the shape of the inward tail of the distribution.

If the number of links is greater than 3, or there are intrinsic kinks in the molecule, the direct determination of the

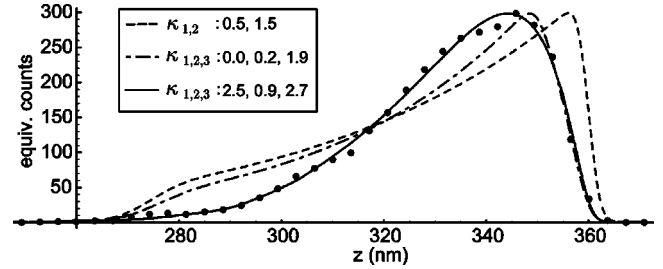


FIG. 9. Tether-only line profile as in Fig. 8, together with least-squares fits for fixed link lengths. For the two-link model (dashed) $(l_1, l_2) = (110, 250)$ nm while for the three-link model $(l_1, l_2, l_3) = (10, 100, 250)$ nm (dash-dotted) and $(l_1, l_2) = (50, 60)$ nm (solid line). The bead radius was 250 nm. Fitted bending stiffnesses are given in $k_B T / \text{rad}$.

transformation T becomes unwieldy. One can then resort to Monte Carlo methods, most conveniently within the rigid-body formalism [17] described above, or to efficient convolution techniques [24]. However, it seems difficult to obtain a large number of relevant twist and bending stiffnesses simultaneously from a measurement of the bead position alone.

The question arises whether standard polymer models would suffice to interpret our data. For a *freely jointed chain*, i.e., a chain of rigid links with no bending potentials, elasticity is purely entropic. This leads to an end-to-end point distribution of the polymer which is peaked at zero extension. With a bead attached, one would find radial profiles that are peaked at the minimum z value, in disagreement with our data. Rather, Figs. 5 and 2 resemble the radial end-to-end PDF [25] and the 2D densities of a *wormlike chain* polymer [26], respectively. Furthermore, in an overstretching experiment on myosin-II [27], an effective persistence length of $l_p = 25 \pm 10$ nm for the coiled-coil tail was found. However, the molecule was deliberately unfolded by the AFM cantilever, so native state elasticity could not be measured. A pure WLC model for the whole MT seems insufficient in our system: even for a WLC attached to a bead, the bead radius constitutes one rigid link of a length comparable to the WLC contour length, which strongly affects the resulting bead center distribution. Our approach constitutes the limit of long segment persistence lengths of a more involved combined segmental-semiflexible description [28].

To further test how well the segmental model describes the experiment, it is desirable to also measure lateral profiles of the bead center histograms. The model should then allow consistent fits of the radial and lateral profiles. A wider lateral observation range may be accomplished by a trapping lens with lower aperture or by lateral stepping of the PFM trap. When the bead size is varied, the bead position histograms should vary with consistent fitted values for (l_1, l_2) and $\{\kappa_i\}$. Generally, with decreasing bead size the value of κ_3 loses importance for the bead histograms, so smaller beads will allow more robust measurement of molecular properties.

VII. CONCLUSION

We have presented a classical statistical mechanics model for the passive elasticity of a single rodlike macromolecule,

assuming that it bends at pointlike joints connecting rigid segments. In combination with fast 3D measurements of bead histograms, this opens the possibility of extracting parameters of passive molecular elasticity in greater detail than was previously possible, and with no other prior information required. In this way bending stiffnesses of the joint regions and the location of the molecular hinge point can be measured even though the bead may be much larger than the molecule itself. The technique is sensitive on a scale of $(0.1\text{--}10)k_B T$ that is difficult to resolve via AFM, and

achieves a spatial resolution of a few nanometers at sampling rates above 200 kHz, under physiological conditions. We believe our combined approach to have great potential for characterizing single macromolecules as entropic-enthalpic springs.

ACKNOWLEDGMENT

We would like to thank Jim Swoger for a thorough reading of the manuscript.

-
- [1] K. Svoboda, P. P. Mitra, and S. M. Block, *Proc. Natl. Acad. Sci. U.S.A.* **91**, 11782 (1994).
 - [2] C. Veigel, M. L. Bartoo, D. C. S. White, J. C. Sparrow, and J. E. Molloy, *Biophys. J.* **75**, 1424 (1998).
 - [3] K. Visscher, M. J. Schnitzer, and S. M. Block, *Nature (London)* **400**, 184 (1999).
 - [4] A. Huxley, *J. Biomech.* **33**, 1189 (2000).
 - [5] A. Vilfan and T. Duke, *Biophys. J.* **85**, 818 (2003).
 - [6] S. Jeney, E. L. Florin, and J. K. H. Hörber, *Methods Mol. Biol.* **164**, 91 (2001).
 - [7] A. Pralle, M. Prummer, E. L. Florin, E. H. K. Stelzer, and J. K. H. Hörber, *Microsc. Res. Tech.* **44**, 378 (1999).
 - [8] A. Rohrbach, C. Tischer, D. Neumayer, E. L. Florin, and E. H. K. Stelzer, *Rev. Sci. Instrum.* **75**, 2197 (2004).
 - [9] M. J. Saxton and K. Jacobson, *Annu. Rev. Biophys. Biomol. Struct.* **26**, 373 (1997).
 - [10] K. Ritchie and A. Kusumi, *Methods Enzymol.* **360**, 618 (2003).
 - [11] M. Speidel, A. Jonas, and E. L. Florin, *Opt. Lett.* **28**, 69 (2003).
 - [12] A. Rohrbach, E. L. Florin, and E. H. K. Stelzer, in *Proceedings of the SPIE in Photon Migration, Optical Coherence Tomography, and Microscopy*, edited by S. Andersson-Engels and M. F. Kaschke (SPIE, Bellingham, WA, 2001), Vol. 4431, pp. 75-86.
 - [13] O. Kratky and G. Porod, *Recl. Trav. Chim. Pays-Bas* **68**, 1106 (1949).
 - [14] J. Howard, *Mechanics of Motor Proteins and the Cytoskeleton* (Sinauer, Sunderland, MA, 2001).
 - [15] C. K. Mathews and K. van Holde, *Biochemistry* (Benjamin/Cummings, Redwood City, CA, 1990).
 - [16] R. Ossig, H. D. Schmitt, B. de Groot, D. Riedel, S. Keranen, H. Ronne, H. Grubmüller, and R. Jahn, *EMBO J.* **19**, 6000 (2000).
 - [17] R. Murray, Z. Li, and S. Sastry, *A Mathematical Introduction to Robotic Manipulation* (CRC Press, Boca Raton, FL, 1993).
 - [18] T. Scholz, S. M. Altmann, M. Antognozzi, C. Tischer, J. K. Heinrich Hörber, and B. Brenner, *Biophys. J.* **88**, 360 (2005).
 - [19] Z. Li, *Int. J. Rob. Autom.* **5**, 139 (1990).
 - [20] R. W. Brockett, in *Mathematical Theory of Networks and Systems*, Proceedings of the International Symposium Held at the Ben Gurion University of the Negev, Beer Sheva, June 1983, edited by P. A. Fuhrman (Springer-Verlag, Berlin, 1984), pp. 120-127.
 - [21] A. Rohrbach and E. H. K. Stelzer, *Appl. Opt.* **41**, 2494 (2002).
 - [22] I. Rayment, H. M. Holden, M. Whittaker, C. B. Yohn, M. Lorenz, K. C. Holmes, and R. A. Milligan, *Science* **261**, 58 (1993).
 - [23] C. Ruff, M. Furch, B. Brenner, D. J. Manstein, and E. Meyerhofer, *Nat. Struct. Biol.* **8**, 226 (2001).
 - [24] G. S. Chirikjian, *Comput. Theor. Polym. Sci.* **11**, 143 (2001).
 - [25] J. Wilhelm and E. Frey, *Phys. Rev. Lett.* **77**, 2581 (1996).
 - [26] G. Lattanzi, T. Munk, and E. Frey, *Phys. Rev. E* **69**, 021801 (2004).
 - [27] I. Schwaiger, C. Sattler, D. R. Hostetter, and M. Rief, *Nat. Mater.* **1**, 232 (2002).
 - [28] Y. Zhou and G. S. Chirikjian, *J. Chem. Phys.* **119**, 4962 (2003).